Available online at www.sciencedirect.com
SCIENCE DIRECT®
Journal of Computational Physics 194 (2004) 659–676
JOURNAL OF COMPUTATIONAL PHYSICS
www.elsevier.com/locate/jcp

# An integral for FHNC calculations

Gary G. Hoffman *

*Department of Chemistry and Biochemistry, Elizabethtown College, Elizabethtown, PA 17022, USA*

Received 4 June 2003; received in revised form 25 August 2003; accepted 25 September 2003

**Abstract**

In considering a modified approximation scheme for Fermi hypernetted chain (FHNC) theory, an integral arose that needed to be evaluated on a routine basis. By evaluating a portion of the integral in closed form, the time required for computation of the complete integral was considerably reduced. This paper presents the closed form evaluation along with some calculations using the result on the electron gas.


*AMS:* 65Z05; 81V70

*Keywords:* Fermi hypernetted chain theory; Fermi cancellation phenomenon; Elementary diagrams

## 1. Introduction

Fermi hypernetted chain (FHNC) theory was originally developed [1–4] for the study of nuclear matter. It was not long, however, before it was recognized as a potentially useful tool for studying other many-fermion systems as well. For instance, the theory has been applied to quantum liquids (such as $^3$He [5–7]) and the fractional quantum Hall effect [8–10]. Of particular interest to the author is the application of FHNC theory to the electronic structure of chemical systems. The theory has been applied to the electron gas [11–13], the charged impurity [14,15], and some closed-shell atoms [16,17]. As a routine computational tool, FHNC theory would certainly be a poor choice. However, circumstances can arise where traditional calculational techniques lead to inconclusive results. FHNC theory provides an alternative, highly accurate approach for the study of many-electron systems and could be used to help resolve questions that may arise in such situations.

The basis of FHNC theory is the assumption of a Jastrow–Feenberg [18] form for the trial wave function. This function consists of a Slater determinant of one-particle functions times a correlation factor. In its usual formulation, the correlation factor is constructed from one-particle and two-particle correlation potentials. The usefulness of the FHNC equations is that they provide a means of evaluating the distri-

* Tel.: +717-361-1241.
*E-mail address:* hoffmang@etown.edu.

0021-9991/$ - see front matter 
doi:10.1016/j.jcp.2003.09.009

bution functions associated with the Jastrow–Feenberg wave function, which in turn can be applied to the evaluation of the expectation value of the hamiltonian. Nearly all efforts in the literature have been aimed at the two-body distribution function although recent work [19] has presented the equations for the three-body distribution. The distribution function is expanded in an infinite sum of terms and a diagrammatic representation of the terms is introduced. These diagrams contain points, which represent particle coordinates, and lines of connection between the points, which represent specific functions. The diagrams can be categorized into several different types and the expansion of the distribution function is separated into several different infinite sums of diagrams. By performing a topological analysis, relationships between the various infinite sums of diagrams can be derived. These are the FHNC equations. The interested reader is directed to the literature [1–4,19–21] for details.

There is one quantity that cannot be provided by the FHNC equations and that must be computed separately. This is the sum of what are known as elementary diagrams. This is an infinite sum and, naturally, only a finite number can be practically evaluated. Some choice of which diagrams are to be incorporated must be made. The most common choice, referred to as the FHNC/0 approximation, is to include no elementary diagrams. The name for this approximation comes from the fact that it includes all elementary diagrams containing up to 0 points. The smallest elementary diagrams contain four points and including all 35 such diagrams [22] is referred to as the FHNC/4 approximation. Naturally, evaluation of 35 terms can be considerably time-consuming and calculations rarely go beyond the FHNC/0 level.

There is another problem with the FHNC/*n* approximations. These choices of elementary diagrams destroy what is known as the fermi cancellation phenomenon. In the sum of diagrams, there are certain groups of terms that exactly cancel each other. This cancellation is associated with the fermi statistics of the particles and is expected to be important for long-range correlations. Krotscheck and Ristig [3,4] first noticed this property of the FHNC/*n* approximation and derived an alternative formulation of the theory that preserves the fermi cancellation phenomenon at all orders of approximation. This is at the expense, however, of neglecting certain contributions to the full cluster expansion. The Krotscheck–Ristig formulation is therefore, at its core, an approximation, and has been referred to "as an incomplete version" [20] of FHNC theory. It would be desirable to deal with the fermi cancellation phenomenon without resorting to a fundamentally approximate formulation. It was this idea that led up to the work reported in this paper.

An explicit example of the problem is given in the following. There are several conventions used to represent the diagrams. The convention used here is that of Gaudin et al. [23]. In the FHNC/0 approximation, the terms

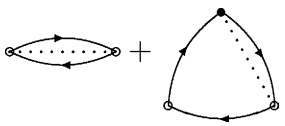

(A)

appear. However, these are canceled by the term

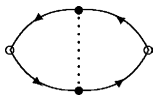

(B)

which does not appear until a higher level of approximation. One thing that the canceling terms have in common is the same number of bond lines (the dotted lines in the diagrams above). The various levels of FHNC/*n* approximation are based instead on the number of points in the elementary diagrams. It seemed reasonable, then, to base the choice of elementary diagrams on the number of bond lines and it is suggested that this might reduce some of the problems that might be associated with a lack of fermi cancellation. Such approximations will be indicated as FHNC(*n*) approximations, the value of *n* indicating the number of bond lines to include in the sum of elementary diagrams.

In the derivation of the FHNC equations, there is one diagram that is technically classified as elementary but is automatically included in the equations and segregated from the rest of the elementary diagrams. This elementary diagram consists solely of a bond line between the two external points. The lowest order approximation based on bond lines should therefore contain all elementary diagrams with one bond line, the so-called FHNC(1) approximation. As it turns out, there is only one such elementary diagram and it is the one given in (B).

It is important to point out that including this diagram does not ensure complete fermi cancellation. Rather, it relegates it to a higher order (but more efficiently than the FHNC/4 approximation would). For instance, in the FHNC(1) approximation, the diagram

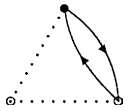

(C)

is included, but the canceling diagram

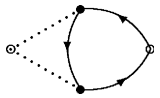

(D)

is not. Diagram (D) is an elementary diagram and would not be included until the FHNC(2) level of approximation (for which there are 20 elementary diagrams).

The project undertaken was to study the FHNC(1) approximation and compare results under this approximation with others. The testing ground for this was chosen to be the electron gas. This requires the evaluation of the integral associated with diagram (B) and this proved to be a difficulty in a number of ways when a fully numerical evaluation was performed. To solve some of the problems, the integral was evaluated partially in closed form and the closed-form evaluation is the subject of this paper. The evaluation is non-trivial and could provide some insights for the evaluation of similar integrals in the application of FHNC theory. Analysis of the FHNC(1) approximation itself is intended for a future publication.

For a homogeneous system, the diagram (B) can be expressed in terms of a many-dimensional integral

$$E_{ee}^{(1)}(r_{12}) = -\frac{1}{8}\rho_0^2 \int \mathrm{d}^3 r\, h(r) \int \mathrm{d}^3 r'\, \sigma(r')\sigma(|\mathbf{r}' - \mathbf{r}_{12}|)\sigma(|\mathbf{r} + \mathbf{r}'|)\sigma(|\mathbf{r} + \mathbf{r}' - \mathbf{r}_{12}|). \tag{1}$$

In this equation, $h(r)$ represents the bond line and is given explicitly by

$$h(r) = \mathrm{e}^{u_2(r)} - 1, \tag{2}$$

where $u_2(r)$ is the two-body correlation potential. The function, $\sigma(r)$, represents the exchange lines (the arrows in the diagram). For a homogeneous system, it is given explicitly by

$$\sigma(r) = \frac{3j_1(k_\mathrm{F} r)}{k_\mathrm{F} r} \tag{3}$$

with $j_1(z)$ being a spherical bessel function of order 1 and $k_\mathrm{F}$ is the fermi wave vector. The fermi wave vector is related to the electron gas density, $\rho_0$, by

$$\rho_0 = \frac{k_\mathrm{F}^3}{3\pi^2}. \tag{4}$$

In a numerical solution of the FHNC equations, the many-dimensional integral (1) must be evaluated over a grid of values of $r_{12}$ and this evaluation would be repeated as the two-body correlation potential was

varied during its optimization. There are certainly numerical techniques that can be used to evaluate this integral, but any analytical reduction would make the evaluation more efficient and more accurate. This reduction is the focus of this paper.

## 2. Reduction of the integral

By introducing the fourier transforms of the exchange line functions, Eq. (1) can be rearranged to

$$E_{ee}^{(1)}(r) = -\frac{81\rho_0^2}{64k_F^{12}} \int_0^\infty \mathrm{d}r'' \, r''^2 h(r'') \int \mathrm{d}^3 q \, j_0(qr'') |F(\mathbf{q}, \mathbf{r})|^2, \tag{5}$$

where

$$F(\mathbf{q}, \mathbf{r}) = \int \mathrm{d}^3 k \, \mathrm{e}^{\mathrm{i}\mathbf{k}\cdot\mathbf{r}} \theta(k_F - k) \theta(k_F - |\mathbf{q} - \mathbf{k}|) \tag{6}$$

and $\theta(z)$ is the heaviside function. It may be mentioned that a different evaluation of the fourier transform of Eq. (5) has been presented in the literature [24]. However, that evaluation relied on an approximate evaluation of Eq. (6) followed by subsequent numerical integrations. The evaluation in this paper relies on no such approximations and so is expected to be more generally useful. A little more manipulation of Eq. (5) leads to

$$\begin{aligned} E_{ee}^{(1)}(r) = & -\frac{81\rho_0^2}{64k_F^{12}} \int_0^\infty \mathrm{d}r'' \, r''^2 h(r'') \int \mathrm{d}^3 k \, \mathrm{e}^{\mathrm{i}\mathbf{k}\cdot\mathbf{r}} \theta(k_F - k) \int \mathrm{d}^3 k' \, \mathrm{e}^{\mathrm{i}\mathbf{k}'\cdot\mathbf{r}} \theta(k_F - k') \\ & \times \int_0^\infty q^2 \, \mathrm{d}q \, j_0(qr'') \int \mathrm{d}\Omega_q \, \theta(k_F - |\mathbf{q} - \mathbf{k}|) \theta(k_F - |\mathbf{q} - \mathbf{k}'|). \end{aligned} \tag{7}$$

The bulk of this paper will focus on the evaluation of the quantity

$$J(q, k, k', \eta) = \int \mathrm{d}\Omega_q \, \theta(k_F - |\mathbf{q} - \mathbf{k}|) \theta(k_F - |\mathbf{q} - \mathbf{k}'|), \tag{8}$$

where $\eta = \cos\theta$, $\theta$ being the angle between the two vectors, $\mathbf{k}$ and $\mathbf{k}'$. That it will depend on only the four coordinates specified can be shown by symmetry arguments. Before getting to this evaluation, consider the reduction of the rest of the integral.

The function, $h(r)$, is assumed to be given. It is therefore possible to evaluate the function

$$\hat{h}(q) = \int_0^\infty r^2 j_0(qr) h(r) \, \mathrm{d}r \tag{9}$$

to a high degree of accuracy. Inserting this into Eq. (7),

$$E_{ee}^{(1)}(r) = -\frac{81\pi^2\rho_0^2}{8k_F^{12}} \int_0^{k_F} \mathrm{d}k \, k^2 \int_0^{k_F} \mathrm{d}k' \, k'^2 \int_{-1}^1 \mathrm{d}\eta \, j_0\left( \left[ k^2 + 2kk'\eta + k'^2 \right]^{1/2} r \right) \int_0^\infty q^2 \, \mathrm{d}q J(q, k, k', \eta) \hat{h}(q). \tag{10}$$

Finally, define the function

$$K(k, k', \eta) = k^2 k'^2 \int_0^\infty q^2 \, \mathrm{d}q J(q, k, k', \eta) \hat{h}(q). \tag{11}$$

The equation for the elementary diagram is then

$$E_{ee}^{(1)}(r) = -\frac{81\pi^2\rho_0^2}{8k_{\mathrm{F}}^{12}} \int_0^{k_{\mathrm{F}}} \mathrm{d}k \int_0^{k_{\mathrm{F}}} \mathrm{d}k' \int_{-1}^{1} \mathrm{d}\eta\, j_0\left(\left[k^2 + 2kk'\eta + k'^2\right]^{1/2} r\right) K(k,k',\eta). \tag{12}$$

The computational procedure is to first evaluate $\hat{h}(q)$ numerically, then using an analytic expression for $J(q,k,k',\eta)$, the function $K(k,k',\eta)$ is evaluated over the appropriate grid. Storing this function, it can be used without change for all values of $r$.

## 3. The evaluation of $J$

The integral in Eq. (8) represents the surface area of that portion of a sphere of radius $q$ centered at the origin which is inside the intersection of two spheres of radius $k_{\mathrm{F}}$ centered at the two points, $\mathbf{k}$ and $\mathbf{k}'$. For clarity, the sphere about the origin which is being integrated over will be referred to as the $q$-sphere, while the other two spheres will be referred to as $k$-spheres. When more specificity is needed, they will be referred to separately as the $k$- and the $k'$-spheres. The magnitudes of the vectors pointing to the centers of the two $k$-spheres are limited in the integrals to a maximum of $k_{\mathrm{F}}$. Therefore, the origin in $\mathbf{q}$ will necessarily be contained in both $k$-spheres. For convenience, let $\mathbf{k}$ correspond to the longer of the two vectors and define the $q_z$-axis so that it is aligned with this vector. Next, define the $q_x$-axis so that $\mathbf{k}'$ is in the $(q_x, q_z)$-plane and has a non-negative component in the $q_x$ direction.

Let $k$, $k'$, and $\eta$ be fixed and consider the evaluation of $J$ over a range of values of $q$. Just how the integrals are to be evaluated depends on the size of $q$. The important issues are associated with how the three spheres intersect each other. To illustrate this, Fig. 1 shows the different ways that the spheres can intersect. The diagrams are the cross sections in the $(q_x, q_z)$-plane with $\mathbf{k} = (0.0, 0.0, 0.9)$, $\mathbf{k}' = (0.4, 0.0, -0.3)$, and $k_{\mathrm{F}} = 1.5$. The $k$-spheres are shown with solid curves and the $q$-sphere with a dashed curve. The dotted lines indicate the projections of where the $q$-sphere intersects the two $k$-spheres; these intersections are actually circles perpendicular to and bisected by the $(q_x, q_z)$-plane that is shown. The hashed region indicates the projection of the surface of the $q$-sphere over which the integration is to be performed. For the smallest value of $q$ shown, the $q$-sphere does not intersect either of the two $k$-spheres and the entire sphere is integrated over. For the second value of $q$, there is one intersection and the integration is over a truncated sphere. For the last two values of $q$, the $q$-sphere intersects both $k$-spheres, but the region of integration is quite different in the two cases. The evaluation of $J$ has to be considered separately in all the different regions.

If $q \leqslant k_{\mathrm{F}} - k$ (recalling that $k$ is the longer of the two vectors), then the $q$-sphere does not intersect either of the $k$-spheres and the evaluation of $J$ is trivial.

$$J(q,k,k',\eta) = 4\pi, \quad q \leqslant k_{\mathrm{F}} - k. \tag{13}$$

If $k_{\mathrm{F}} - k \leqslant q \leqslant k_{\mathrm{F}} - k'$, then the $q$-sphere intersects only the $k$-sphere centered at $\mathbf{k}$ and again, the integral is trivial.

$$J(q,k,k',\eta) = 2\pi(1 - \cos\alpha) \quad k_{\mathrm{F}} - k \leqslant q \leqslant k_{\mathrm{F}} - k', \tag{14}$$

where $\alpha$ is the angle between $\mathbf{k}$ and the point on the $q$-sphere at which the intersection occurs. Specifically,

$$\cos\alpha = \frac{k^2 + q^2 - k_{\mathrm{F}}^2}{2qk}. \tag{15}$$

At the other extreme, if $q \geqslant k_{\mathrm{F}} + k'$ then the surface of the $q$-sphere is outside the region of intersection of the two $k$-spheres and clearly,

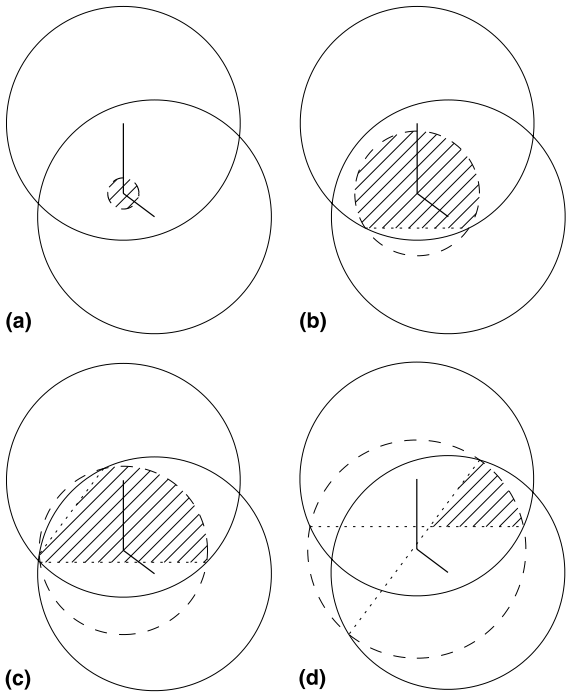


Fig. 1. The intersection of spheres in a typical case for several values of $q$. All cases have $k = 0.9$, $k' = 0.5$, $\eta = -0.6$, and $k_F = 1.5$. The values of $q$ are: (a) $q = 0.2$, (b) $q = 0.8$, (c) $q = 1.08$, and (d) $q = 1.4$. The spheres about the two points are shown with solid curves and that about the origin with a dashed curve. The spheres intersect at the dashed lines and the region over which the integrals must be performed is indicated by the hashes.

$$J(q,k,k',\eta) = 0, \quad q \geqslant k_F + k'. \tag{16}$$

For the other values of $q$, the situation is more complicated. Viewing the projections in the $(q_x, q_z)$-plane is helpful for organizing the various cases that must be considered. These projections are best represented with the $q$-sphere appearing as a circle and the projections of the intersections with the $k$-spheres appearing as lines. The vectors, $\mathbf{k}$ and $\mathbf{k}'$, are viewed as given quantities and the $q$-sphere is allowed to grow in size, the intersections with the $k$-spheres being introduced at the appropriate times.

Keep in mind that $k \geqslant k'$, that $\mathbf{k}$ is directed along the positive $q_z$-axis, and that $\mathbf{k}'$ is directed in the positive $q_x$ half-plane (unless it points along the $q_z$-axis). These facts allow several general features to be identified. First, as $q$ increases in magnitude from 0, the intersection with the $k$-sphere occurs first, starting when $q = k_F - k$. The projection of this intersection will appear first as a point at the very bottom of the $q$-sphere and then as a rising horizontal line. Trigonometric analysis leads to the following equation for this line

$$q_z = z_0 \equiv q\cos\alpha = \frac{k^2 + q^2 - k_F^2}{2k}, \tag{17}$$

where $q_z$ represents the $z$-coordinate in the $(q_x, q_z)$-plane. The projection of the surface of the $q$-sphere over which the integration in $J$ is to be performed will be above this horizontal line.

The $q$-sphere first intersects the $k'$-sphere when $q = k_F - k'$. It appears as a point at an angle $\pi - \theta$ with the vertical and to the left of the $q_z$-axis ($\theta$, recall, is the angle between $\mathbf{k}$ and $\mathbf{k}'$). It will be exactly opposite

to the direction in which $\mathbf{k}'$ is pointing. As $q$ grows, the point grows to a line, always perpendicular to the vector $\mathbf{k}'$. It moves in the direction of the $\mathbf{k}'$ vector as $q$ grows. The equation for this line is given by

$$q_z = z_1 + \frac{(z_2 - z_1)}{(x_2 - x_1)}\,(q_x - x_1), \tag{18}$$

where $q_x$ and $q_z$ are the coordinates in the $(q_x, q_z)$-plane. The various parameters appearing are the points on the $q$-sphere at which it intersects the $k'$-sphere. Trigonometric analysis leads to the formulas

$$\begin{aligned} x_1 &= q\{\sin\theta\cos\alpha' - \cos\theta\sin\alpha'\},\\ x_2 &= q\{\sin\theta\cos\alpha' + \cos\theta\sin\alpha'\},\\ z_1 &= q\{\cos\theta\cos\alpha' + \sin\theta\sin\alpha'\},\\ z_2 &= q\{\cos\theta\cos\alpha' - \sin\theta\sin\alpha'\} \end{aligned} \tag{19}$$

and $\alpha'$ is the angle between $\mathbf{k}'$ and where the $k'$-sphere intersects the $q$-sphere. Specifically,

$$\cos\alpha' = \frac{k'^2 + q^2 - k_{\mathrm{F}}^2}{2qk'}. \tag{20}$$

If $x_2 = x_1$, Eq. (18) is not defined. This case corresponds to the intersection being a vertical line. The correct equation to use in this case is

$$q_x = x_1. \tag{21}$$

The projection of the surface over which the integration in $J$ is to be performed will be to the right of the intersection line with the $k'$-sphere. If $\theta$ equals 0 or $\pi$, the projection will be above or below, respectively.

Fig. 2 illustrates the various geometrical quantities that have been defined. It shows the projection of the intersecting spheres in the $(q_x, q_z)$-plane. The $q$-sphere appears as a circle and the intersections with the $k$- and $k'$-spheres appear as chords in the circle. The vectors $\mathbf{k}$ and $\mathbf{k}'$ are also shown. Three angles have been defined and they are illustrated in the figure. The angle between the two vectors $\mathbf{k}$ and $\mathbf{k}'$ is defined as $\theta$. The angle $\alpha$ is defined as the angle between $\mathbf{k}$ and the line from the center of the $q$-sphere to where the $k$-sphere intersects the $q$-sphere. The angle $\alpha'$ is defined similarly with respect to the vector $\mathbf{k}'$. The points in the $(q_x, q_z)$-plane where the $k$-sphere intersects the $q$-sphere occur at $(x_\pm, z_0) = (\pm q\sin\alpha, q\cos\alpha)$. The points in the $(q_x, q_z)$-plane, where the $k'$-sphere intersects the $q$-sphere occur at $(x_1, z_1)$ and $(x_2, z_2)$, where the coordinates are defined in Eq. (19).

The evaluation of $J$ depends critically on whether the two lines of intersection cross within the circle for the $q$-sphere or not. If they do not intersect, the integrations are not difficult. When the $k'$-sphere is first intersected, the point of intersection may either be above or below the line of intersection with the $k$-sphere. The point then grows into a line and at some point it meets the other line of intersection at the perimeter of the $q$-sphere. In this interval of $q$ values, the region of integration is equal to the surface area of the $q$-sphere minus only the cap below the line for the $k$-sphere intersection if the intersection with the $k'$-sphere is below this intersection line. If the $k'$-sphere intersection line is above that for the $k$-sphere, then a second spherical cap must be subtracted. These two situations are illustrated in Fig. 3. Which situation applies can be determined by considering what happens when the $q$-sphere first intersects the $k'$-sphere. This occurs when $q = k_{\mathrm{F}} - k'$ and the two spheres just touch at an angle $\pi - \theta$ from the vertical. The intersection with the $k'$-sphere is below that for the $k$-sphere if

$$\cos(\pi - \theta) = -\cos\theta < \cos\alpha = \frac{k^2 + k'^2 - 2k_{\mathrm{F}}k'}{2k(k_{\mathrm{F}} - k')}. \tag{22}$$

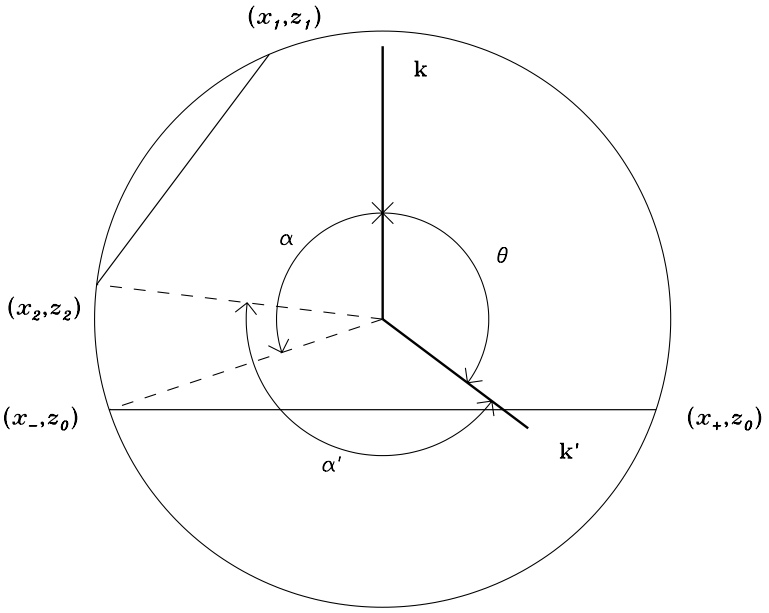


Fig. 2. A view of the $q$-sphere projected in the $(q_x, q_z)$-plane along with the various geometric quantities defined in the text.

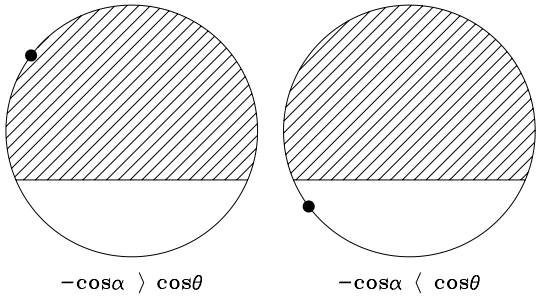


Fig. 3. The two situations where the intersection with the $k'$-sphere is above or below that with the $k$-sphere.

The intersection is above if the inequality is reversed. The evaluation of $J$ in the region before the two lines intersect within the sphere is then given by

$$J = \begin{cases} 2\pi(1-\cos\alpha) = \dfrac{\pi(k_F^2 - (k-q)^2)}{kq}, & -\cos\theta < \cos\alpha, \\ -2\pi(\cos\alpha + \cos\alpha') = \dfrac{\pi(k+k')(k_F^2 - q^2 - kk')}{qkk'}, & -\cos\theta > \cos\alpha. \end{cases} \tag{23}$$

From Fig. 2, it can be deduced that the two lines first intersect when $\theta + \alpha + \alpha' = 2\pi$. Insertion of the various quantities and solving for $q$ leads to two solutions.

$$q_\pm = \left[ k_F^2 + kk' \left( \cos\theta \pm \left[ \frac{4k_F^2}{k^2 - 2kk'\cos\theta + k'^2} - 1 \right]^{1/2} \sin\theta \right) \right]^{1/2}. \tag{24}$$

The lower sign corresponds to the desired root. The upper sign represents the value of $q$ where the two lines just intersect on the right side of the circle. This is illustrated in Fig. 4 for the two cases where the intersection with the $k'$-sphere first occurs above or below that with the $k$-sphere. Eq. (23) is applicable for $k_F - k' < q < q_-$.

For the region $q_- < q < q_+$, the two lines intersect within the $q$-sphere and the integration is more complicated. Fortunately, the integration can be decomposed into several contributions for which Lustig [25] has provided analytic formulas. Lustig derived a formula for the surface area of what he calls a *diangle*. A diangle is the portion of a sphere obtained by cutting the sphere exactly in half and then once more in an arbitrary plane. It is necessary only to identify the appropriate diangles that are combined in the evaluation of $J$ and perform the necessary algebra on the result.

To be clear on notation, consider the diangle represented in Fig. 5. Note first that the division of the sphere by the two planes actually generates four diangles. Attention will always be focused on the smaller side of the second plane – the one *not* going through the center of the sphere. There are two such diangles on this side. Fig. 5 represents the plane through the center of the sphere and perpendicular to the two dividing planes. Orient the planes so that the second plane is horizontal and the diangle is the right-most portion above the second plane. Two angles can then be identified: $\chi$ represents the angle between the vertical and the plane passing through the center of the sphere and $\psi$ represents the angle between the vertical and the line from the center of the sphere to where the second plane intersects the sphere. The angle $\chi$ will be considered positive if it is to the right of the vertical (towards the region of the diangle) and negative if it is to the left (where the diangle now extends beyond the vertical). The angle $\psi$ is always positive. It is easily deduced that $\chi$ extends from $-\pi/2$ to $\pi/2$ and $\psi$ extends from 0 to $\pi/2$. For $\chi > 0$, the formula of Lustig [25] gives the surface area

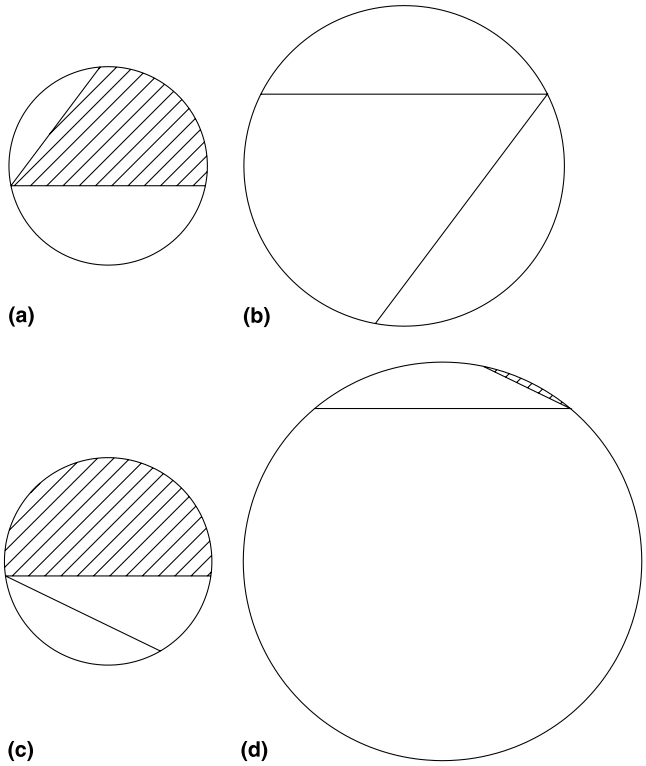


Fig. 4. The points where the two lines just intersect with the $q$-sphere. The left-hand figures correspond to $q_-$ and the right-hand figures to $q_+$ of Eq. (24).

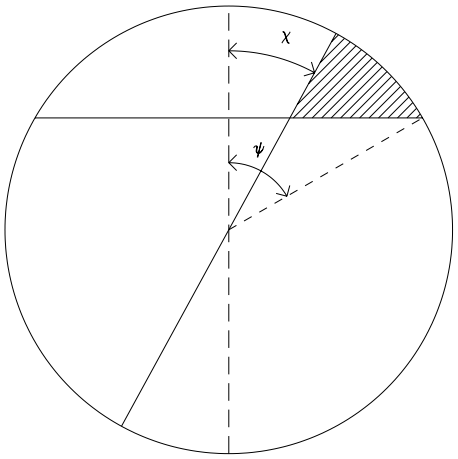


Fig. 5. The definitions of the angles $\chi$ and $\psi$ used for the evaluation of the surface area over a diangle.

$$S(\sin\chi,\sin\psi)=2\left\{\arcsin\left(\left[1-\frac{\sin^2\chi}{\sin^2\psi}\right]^{1/2}\right)-\cos\psi\arccos\left(\frac{\tan\chi}{\tan\psi}\right)\right\}\quad(\chi>0). \tag{25}$$

If $\chi<0$, the formula of Lustig must be modified. It can be shown that

$$S(\sin\chi,\sin\psi)=2\left\{\pi-\arcsin\left(\left[1-\frac{\sin^2\chi}{\sin^2\psi}\right]^{1/2}\right)-\cos\psi\arccos\left(\frac{\tan\chi}{\tan\psi}\right)\right\}\quad(\chi<0). \tag{26}$$

Eqs. (25) and (26) can be combined into the single equation

$$S(\sin\chi,\sin\psi)=2\left\{\arccos\left(\frac{\sin\chi}{\sin\psi}\right)-\cos\psi\arccos\left(\frac{\tan\chi}{\tan\psi}\right)\right\}. \tag{27}$$

Since Eq. (27) assumes that the diangle of interest is on the smaller side of the second cutting plane, its use will depend on the relationship between the angles $\alpha$ and $\alpha'$. Since $k\geqslant k'$, it is always true that $\cos\alpha\geqslant\cos\alpha'$. Where the diangles for which Eq. (27) can be applied occur depends on whether these cosines are greater than or less than 0. There are three separate cases to consider: (*a*) $\cos\alpha'\leqslant\cos\alpha\leqslant 0$, (*b*) $\cos\alpha'\leqslant 0\leqslant\cos\alpha$, and (*c*) $0\leqslant\cos\alpha'\leqslant\cos\alpha$.

Consider case *a* first. A typical scenario is illustrated in Fig. 6. The region over which $J$ is to be evaluated is above the horizontal line and to the right of the second line. This is best evaluated by subtracting from the full surface area of the sphere the areas of the two spherical caps and then adding back the area for the overlapping region of the two caps. It is this overlapping area to which Eq. (27) can be applied.

This region is composed of two diangles. Draw a radius through the intersection of the two lines. For the diangle that is shaded in Fig. 6, the angle $\psi$ is given by $\pi-\alpha$. For the other diangle, the angle $\psi$ is given by $\pi-\alpha'$. Focus for now on the shaded diangle. This is constructed with the horizontal line and a perpendicular has been drawn to this line going through the center of the circle. The angle $\chi$ to be used in Eq. (27) corresponds to the angle $\beta$ drawn in the figure. A perpendicular is also drawn with the other line and the four-sided figure constructed from the two perpendiculars and the two lines is reproduced in Fig. 7. The four sides and the two diagonals are labeled. Using a number of trigonometric identities, it is possible to relate the angle $\beta$ to the parameters used to define the original problem.

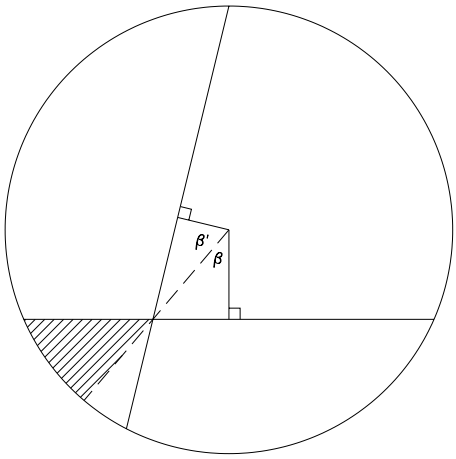


Fig. 6. The geometry associated with case *a*.

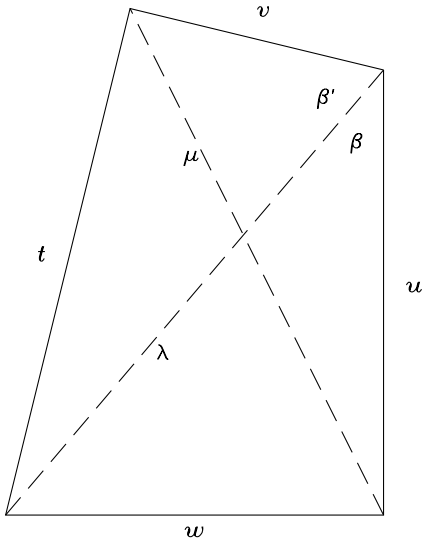


Fig. 7. The four-sided figure associated with Fig. 6.

To begin, the two perpendiculars are collinear with $\mathbf{k}$ and $\mathbf{k}'$, so the angle between them is $\theta$. Next, using the definitions of $\alpha$ and $\alpha'$, the lengths of the perpendiculars are given by $u = q\cos(\pi - \alpha) = -q\cos\alpha$ and $v = -q\cos\alpha'$. The diagonal, $\lambda$, is the common hypotenuse of two right triangles, so that

$$\lambda^2 = u^2 + w^2 = t^2 + v^2. \tag{28}$$

The diagonal, $\mu$, is also common to two triangles. One of the opposite angles is $\theta$. By construction, the other must be $\pi - \theta$. Solving Eq. (28) for $t$ and inserting it into the equation for $\mu$, there results

$$\mu^2 = u^2 + v^2 - 2uv\cos\theta = 2w^2 + u^2 - v^2 + 2w\left[w^2 + u^2 - v^2\right]^{1/2}\cos\theta. \tag{29}$$

Define $\zeta = w^2 - v^2$. Eq. (29) then can be written

$$\zeta^2 \sin^2\theta - (u^2\cos^2\theta - 2uv\cos\theta + v^2\cos^2\theta)\zeta = 0. \tag{30}$$

One solution of this equation is $\zeta = 0$ which implies that $w^2 = v^2$. This is certainly not true in general, so that it is the second solution which is required.

$$\zeta = \frac{u^2\cos^2\theta - 2uv\cos\theta + v^2\cos^2\theta}{\sin^2\theta}. \tag{31}$$

This allows $w$ and $\lambda$ to be evaluated in terms of $u$ and $v$ and there results

$$\sin^2\beta = \frac{w^2}{\lambda^2} = \frac{(v - u\cos\theta)^2}{u^2 - 2uv\cos\theta + v^2} = \frac{(\cos\alpha' - \cos\alpha\cos\theta)^2}{\cos^2\alpha - 2\cos\alpha\cos\alpha'\cos\theta + \cos^2\alpha'}. \tag{32}$$

The correct sign is obtained with the root

$$\sin\beta = \frac{\cos\alpha\cos\theta - \cos\alpha'}{[\cos^2\alpha - 2\cos\alpha\cos\alpha'\cos\theta + \cos^2\alpha']^{1/2}}. \tag{33}$$

Since $\beta' = \theta - \beta$ and $\beta \leqslant \pi/2$, it can be shown immediately that

$$\sin\beta' = \frac{\cos\alpha'\cos\theta - \cos\alpha}{[\cos^2\alpha - 2\cos\alpha\cos\alpha'\cos\theta + \cos^2\alpha']^{1/2}}. \tag{34}$$

Although $\sin\beta$ can never be negative (since $\cos\alpha' \leqslant \cos\alpha \leqslant 0$), the quantity $\sin\beta'$ can be. The evaluation of $J$ for case $a$ is therefore given by

$$J = -2\pi(\cos\alpha + \cos\alpha') + S(\sin\beta, \sin\alpha) + S(\sin\beta', \sin\alpha') \quad (\cos\alpha \leqslant 0). \tag{35}$$

Case $b$ corresponds to $\cos\alpha' \leqslant 0 \leqslant \cos\alpha$. A typical scenario is illustrated in Fig. 8. The region over which the integral is to be performed is above the horizontal line and to the right of the other. It is more convenient here to evaluate $J$ directly. Because of the arrangement of the lines, the evaluation of $J$ corresponds to a difference of diangle areas. The first diangle is that fully to the right of the dashed line in Fig. 8 and

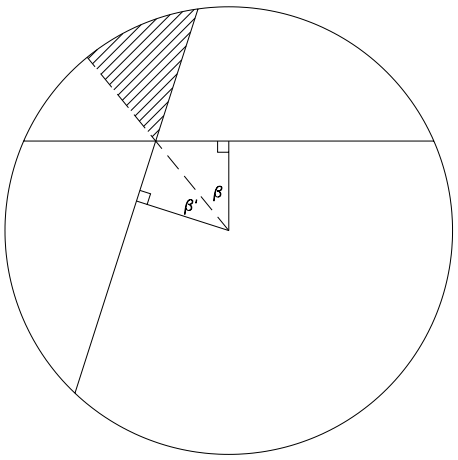


Fig. 8. The geometry associated with case $b$.

above the horizontal line. From the area of this diangle must be subtracted the area of the diangle marked by the hash marks in the figure. For the larger diangle, the angle $\psi$ corresponds to $\alpha$. The angle $\beta$ can be evaluated in a similar way to the case $a$ analysis except that now $u = q\cos\alpha$ and $v = -q\cos\alpha'$. Following through, it is found that

$$\sin\beta = \frac{\cos\alpha' - \cos\alpha\cos\theta}{\left[\cos^2\alpha - 2\cos\alpha\cos\alpha'\cos\theta + \cos^2\alpha'\right]^{1/2}} \tag{36}$$

and

$$\sin\beta' = \frac{\cos\alpha - \cos\alpha'\cos\theta}{\left[\cos^2\alpha - 2\cos\alpha\cos\alpha'\cos\theta + \cos^2\alpha'\right]^{1/2}}. \tag{37}$$

There results

$$J = S(\sin\beta, \sin\alpha) - S(\sin\beta', \sin\alpha') \quad (\cos\alpha' \leqslant 0 \leqslant \cos\alpha). \tag{38}$$

Case $c$ closely parallels the other two. Eqs. (36) and (37) hold for this case as well and

$$J = S(\sin\beta, \sin\alpha) + S(\sin\beta', \sin\alpha') \quad (0 \leqslant \cos\alpha' \leqslant \cos\alpha). \tag{39}$$

It is desirable to have a common formula for all three cases. The quantities in Eqs. (33) and (34) differ only in sign from those in Eqs. (36) and (37). It is convenient to define the angles, $\gamma$ and $\gamma'$, so that regardless of the conditions,

$$\sin\gamma = \frac{\cos\alpha' - \cos\alpha\cos\theta}{\left[\cos^2\alpha - 2\cos\alpha\cos\alpha'\cos\theta + \cos^2\alpha'\right]^{1/2}} \tag{40}$$

and

$$\sin\gamma' = \frac{\cos\alpha - \cos\alpha'\cos\theta}{\left[\cos^2\alpha - 2\cos\alpha\cos\alpha'\cos\theta + \cos^2\alpha'\right]^{1/2}}. \tag{41}$$

With these definitions, the expressions for the three cases can be worked out in a little more detail.
(a) $\cos\alpha' \leqslant \cos\alpha \leqslant 0$

$$J = 2\left\{\arccos\left(-\frac{\sin\gamma}{\sin\alpha}\right) + \arccos\left(-\frac{\sin\gamma'}{\sin\alpha'}\right) - \cos\alpha\arccos\left(\frac{\tan\gamma}{\tan\alpha}\right) - \cos\alpha'\arccos\left(\frac{\tan\gamma'}{\tan\alpha'}\right)\right\}, \tag{42}$$

(b) $\cos\alpha' \leqslant 0 \leqslant \cos\alpha$

$$J = 2\left\{\arccos\left(\frac{\sin\gamma}{\sin\alpha}\right) - \arccos\left(\frac{\sin\gamma'}{\sin\alpha'}\right) - \cos\alpha\arccos\left(\frac{\tan\gamma}{\tan\alpha}\right) - \cos\alpha'\arccos\left(\frac{\tan\gamma'}{\tan\alpha'}\right)\right\}, \tag{43}$$

(c) $0 \leqslant \cos\alpha' \leqslant \cos\alpha$

$$J = 2\left\{\arccos\left(\frac{\sin\gamma}{\sin\alpha}\right) + \arccos\left(\frac{\sin\gamma'}{\sin\alpha'}\right) - \cos\alpha\arccos\left(\frac{\tan\gamma}{\tan\alpha}\right) - \cos\alpha'\arccos\left(\frac{\tan\gamma'}{\tan\alpha'}\right)\right\}. \tag{44}$$

These three formulas differ only in the first two terms. By introducing an identity for the arccosine [26], the first two terms in all three expressions can be replaced by

$$\text{(Sum of first two terms)} = \arccos\left(\frac{1}{\sin\alpha\sin\alpha'}\left\{\sin\gamma\sin\gamma' - \cos\alpha\cos\alpha'\left[\frac{(\sin^2\alpha-\sin^2\gamma)(\sin^2\alpha'-\sin^2\gamma')}{(1-\sin^2\alpha)(1-\sin^2\alpha')}\right]^{1/2}\right\}\right). \tag{45}$$

Finally, introducing the definitions of $\gamma$ and $\gamma'$ and keeping track of the signs of the trigonometric functions in the three regions, it can be shown that

$$J = 2\left\{\arccos\left(\frac{\cos\alpha\cos\alpha'-\cos\theta}{\sin\alpha\sin\alpha'}\right) - \cos\alpha\arccos\left(\frac{\cos\alpha'-\cos\alpha\cos\theta}{\sin\theta\sin\alpha}\right) - \cos\alpha'\arccos\left(\frac{\cos\alpha-\cos\alpha'\cos\theta}{\sin\theta\sin\alpha'}\right)\right\}. \tag{46}$$

This equation is valid regardless of the relative values of $\cos\alpha$ and $\cos\alpha'$.

There is now one more case that needs to be considered. For smaller values of $\theta$, it is possible for the region excluded by the intersection with the $k'$-sphere to fully contain that for the $k$-sphere. This situation is illustrated in case (d) of Fig. 4. This situation occurs when $\cos\alpha_+ < \cos\theta$, where

$$\cos\alpha_+ = \frac{k^2+q_+^2-k_F^2}{2kq_+}. \tag{47}$$

In such a situation, with $q_+ < q < k_F + k'$,

$$J = 2\pi(1-\cos\alpha') = \frac{\pi(k_F^2-(k'-q)^2)}{k'q}. \tag{48}$$

## 4. Summary

The equations can be summarized as follows.

$$J = \begin{cases} 4\pi & 0 \le q \le k_F - k \\ \frac{\pi(k_F^2-(k-q)^2)}{kq} & k_F - k \le q \le k_F - k' \\ \begin{cases} \frac{\pi(k_F^2-(k-q)^2)}{kq} & -\cos\alpha_- \le \cos\theta \\ \frac{\pi(k+k')(k_F^2-q^2-kk')}{qkk'} & -\cos\alpha_- \ge \cos\theta \end{cases} & k_F - k' \le q \le q_- \\ 2\left\{\arccos\left(\frac{\cos\alpha\cos\alpha'-\cos\theta}{\sin\alpha\sin\alpha'}\right) - \cos\alpha\arccos\left(\frac{\cos\alpha'-\cos\alpha\cos\theta}{\sin\theta\sin\alpha}\right) - \cos\alpha'\arccos\left(\frac{\cos\alpha-\cos\alpha'\cos\theta}{\sin\theta\sin\alpha'}\right)\right\} & q_- \le q \le q_+ \\ \begin{cases} \frac{\pi(k_F^2-(k'-q)^2)}{k'q} & \cos\alpha_+ \le \cos\theta \\ 0 & \cos\alpha_+ \ge \cos\theta \end{cases} & q_+ \le q \le k_F + k' \\ 0 & k_F + k' \le q \end{cases} \tag{49}$$

where the parameters are defined as

Table 1
Computed energies (in hartree atomic units) within the FHNC/0 and FHNC(1) approximations

| $r_s$ | FHNC/0 | FHNC(1) |
|---|---|---|
| 1.0 | 0.58496 | 0.60518 |
| 2.0 | 0.00263 | 0.01246 |
| 3.0 | −0.06488 | −0.05881 |
| 4.0 | −0.07445 | −0.07021 |
| 5.0 | −0.07238 | −0.06919 |
| 6.0 | −0.06771 | −0.06519 |
| 7.0 | −0.06275 | −0.06070 |
| 8.0 | −0.05814 | −0.05643 |
| 9.0 | −0.05402 | −0.05256 |
| 10.0 | −0.05038 | −0.04911 |

$$q_{\pm} = \left[ k_{\mathrm{F}}^2 + kk' \left( \cos\theta \pm \left[ \frac{4k_{\mathrm{F}}^2}{k^2 - 2kk'\cos\theta + k'^2} - 1 \right]^{1/2} \sin\theta \right) \right]^{1/2} \tag{50}$$

and

$$\cos\alpha_{\pm} = \frac{k^2 + q_{\pm}^2 - k_{\mathrm{F}}^2}{2kq_{\pm}}. \tag{51}$$

## 5. FHNC calculations

A program was written to perform the evaluation of Eq. (12). In this program, the function, $u_2(r)$, is given and the fourier transform, $\hat{h}(q)$, defined in Eqs. (9) and (2), is evaluated numerically. This numerical function is then used with the analytically evaluated function, $J(q,k,k',\eta)$, to compute $K(k,k',\eta)$ over a numerical grid. For the values of $r$ over a chosen grid, the three remaining integrations are performed numerically. The technical details are given in Appendix A.

The use of the analytic expression for $J$ was compared with the same calculations performed using a fully numerical algorithm. The use of Eq. (49) required only 12% of the CPU time that the fully numerical calculation did. It was also noted that the use of the analytic expression led to a better behaved result for $E_{ee}^{(1)}(r)$ for larger values of $r$. One of the main reasons for embarking on this evaluation was to assess the usefulness of the FHNC(1) approximation. The total energy of the electron gas for several values of $r_s$ were computed within the FHNC approximation, first with the FHNC/0 approximation (no elementary diagrams), and second with the FHNC(1) approximation (one elementary diagram). The results are given in Table 1. The FHNC(1) energies are all higher than the FHNC/0 energies. Except for the $r_s = 2$ results, they are about 5–10% different; the energy goes through zero near $r_s = 2$, so a percent difference is not very meaningful in this case. Calculations by Zabolitzky [22] on several model potentials indicate comparable differences between the FHNC/0 and FHNC/4 approximations. Unfortunately, he did not consider the electron gas in that study.

## 6. Conclusions

The single-bond elementary diagram of FHNC theory requires the evaluation of a multidimensional integral. A portion of this integral was evaluated in closed form and the result is summarized in Eq.

(49). This is the main result of this paper. The evaluation of this integral may prove useful for similar integrals that appear in FHNC theory. The specific integral evaluated corresponds to a homogeneous system, but it may be desired to apply the FHNC(1) approximation to inhomogeneous many-electron systems. The evaluation outlined here may provide some insights for the more general integral. Higher order approximations, further, may require similar integrations and the evaluation in this paper may provide some assistance in such cases. Calculations with this formula led to a reduction in CPU time by about 88% relative to a fully numerical calculation. The results of these calculations were also better behaved.

One of the driving forces for evaluating this integral was the proposal of an approximate formulation for the FHNC theory which bases the inclusion of the elementary diagrams on the number of bond lines rather than the number of points. The lowest order approximation in this formalism is the FHNC(1) approximation, which incorporates the single-bond elementary diagram into the equations. Calculations on the electron gas at this level of approximation led to differences from the FHNC/0 approximation that are comparable to the differences observed when the FHNC/4 approximation is used in other model systems [22]. These results suggest that the FHNC(1) approximation may yield improvements over the FHNC/0 approximation comparable to those for the FHNC/4 approximation but with much less effort. Further investigation of this is needed.

It is also possible to argue that the FHNC(1) approximation should be used in any event. The fermi cancellation phenomenon is associated with diagrams having the same number of bond lines. It is therefore reasonable to group together diagrams according to the number of bond lines. Since one elementary diagram with a single bond line is automatically incorporated into the FHNC equations, it makes sense to include the other elementary diagram with a single bond line as well. This is another issue that needs further investigation.

A particularly tantalizing idea to which the present work might be applied involves what has been referred to as the "scaling method" for HNC theory [27]. HNC calculations on liquid $^4$He [28] suggest a proportionality of the different order contributions to the sum of elementary diagrams. Based on this observation, the entire sum of elementary diagrams can be proposed to be proportional to the lowest order correction, which happens to be a single diagram with four points. The proportionality constant is determined by enforcing the equivalence of two different expressions for the kinetic energy of the system. These two expressions must be equal when all elementary diagrams are included, but differ when only a finite number of terms are used. One might propose a similar approximation for FHNC theory and this, in fact, was done in [7] for the study of liquid $^3$He. In FHNC theory there are four different types of elementary diagrams that may be collected in a matrix, $\mathbf{E}$. If $\mathbf{E}^{(1)}$ consists of those elementary diagrams that contain only one bond line, the scaling approximation amounts to assuming

$$\mathbf{E} = (1 + s)\mathbf{E}^{(1)}. \tag{52}$$

The scaling factor, $s$, is determined by requiring that, for instance, the Pandharipande–Bethe [29] and Jackson–Feenberg [30] forms for the energy be equal. The assumption (52) differs in detail from that of [7] and further investigation of this idea is called for.

## Acknowledgements

The author wishes to thank one of the reviewers who suggested the scaling approximation as a potential application for the present work.

## Appendix A. Computational details

The evaluation of $E_{ee}^{(1)}(r)$ was carried out in stages. The form for the two-body correlation potential was assumed to be

$$u_2(r) = -\frac{a(1-\mathrm{e}^{-br})}{r} \tag{A.1}$$

with $a$ and $b$ being variational parameters. This is the same type of variational function used by Chakravarty and Woo [31] and others. In order to evaluate the fourier transform, $\hat{h}(q)$, it proved useful to extract the long-range part. Define

$$h^0(r) = \mathrm{e}^{-a/r} - 1. \tag{A.2}$$

A straightforward evaluation of the integral gives

$$\hat{h}^0(q) \equiv \int_0^\infty r^2 j_0(qr) h^0(r)\,\mathrm{d}r = -\frac{2a}{q^2}\,\mathrm{ker}_2(2\sqrt{aq}), \tag{A.3}$$

where $\mathrm{ker}_2(x)$ is the kelvin function of order 2 [32]. The desired function can then be written as

$$q^2\hat{h}(q) = -2a\,\mathrm{ker}_2(2\sqrt{aq}) + q^2\delta\hat{h}(q), \tag{A.4}$$

where

$$\delta\hat{h}(q) = \int_0^\infty r^2 j_0(qr)\left(\mathrm{e}^{-a(1-\mathrm{e}^{-br})/r} - \mathrm{e}^{-a/r}\right)\mathrm{d}r. \tag{A.5}$$

The reason for including the factor of $q^2$ in Eq. (A.4) is to avoid the divergence in $\mathrm{ker}_2(2\sqrt{aq})$ as $q \to 0$. The integral in Eq. (A.5) is easily evaluated numerically. The integrand is short-ranged so that the integration can be truncated at a relatively small value of $r$. The maximum value of $r$ was chosen so that $\mathrm{e}^{-br}$ was insignificant with respect to unity. This was set equal to $-\ln\delta/b$, where $\delta = 10^{-10}$. A 4097-point Romberg integration [33] was used for this evaluation.

The function $K(k,k',\eta)$ was evaluated numerically using a 4097-point Romberg integration. Since $J(q,k,k',\eta)$ vanishes for $q > 2k_\mathrm{F}$, the integration is effectively finite-ranged. This function was evaluated over a grid of 129 values of $\eta$ (from $-1$ to 1) and two grids of 257 points each of $k$ and $k'$. For efficiency, only distinct pairs of $k$ and $k'$ were explicitly evaluated. The resulting function was stored in a grid for use in all the other integrals.

The remaining integrals were performed by successive Romberg integrations of the 129-point $\eta$ grid, the 257-point $k'$ grid, and the 257-point $k$ grid. The FHNC equations were solved for the two-body distribution and the energy evaluated using the Clark–Westhaus [34] form for the kinetic energy and the superposition approximation [35] for the three-body distribution. The integral over $\eta$ was done by Romberg integration over the 129-point grid and the integrals over $k$ and $k'$ were also performed by Romberg integration over the 257-point grids. The programs were written in C and run on a *DEC 600au* personal workstation.

## References

[1] S. Fantoni, S. Rosati, Lett. Nuovo Cimento 10 (1974) 545.
[2] S. Fantoni, S. Rosati, Nuovo Cimento 25A (1975) 593.
[3] E. Krotscheck, M.L. Ristig, Phys. Lett. 48A (1974) 17.
[4] E. Krotscheck, M.L. Ristig, Nucl. Phys. A 242 (1975) 389.

[5] E. Krotscheck, J. Low Temp. Phys. 27 (1977) 199.
[6] J.G. Zabolitzky, Phys. Rev. A 16 (1977) 1258.
[7] E. Manousakis, S. Fantoni, V.R. Pandharipande, Q.N. Usmani, Phys. Rev. B 28 (1983) 3770.
[8] O. Ciftja, S. Fantoni, Phys. Rev. B 56 (1997) 13290.
[9] O. Ciftja, S. Fantoni, Phys. Rev. B 58 (1998) 7898.
[10] O. Ciftja, C. Wexler, Phys. Rev. B 65 (2002) 205307.
[11] L.J. Lantto, Phys. Rev. A 22 (1980) 1380.
[12] J.G. Zabolitzky, Phys. Rev. B 22 (1980) 2353.
[13] E. Krotscheck, Ann. Phys. 155 (1984) 1.
[14] A. Kallio, P. Pietiläinen, L. Lantto, Phys. Scr. 25 (1982) 943.
[15] P. Pietiläinen, A. Kallio, Phys. Rev. B 27 (1983) 224.
[16] T. Pang, C.E. Campbell, E. Krotscheck, Chem. Phys. Lett. 163 (1989) 537.
[17] C.E. Campbell, E. Krotscheck, T. Pang, Phys. Rep. 213 (1992) 1.
[18] E. Feenberg, Theory of Quantum Fluids, Academic Press, New York, 1969.
[19] G.G. Hoffman, Phys. Rev. B 64 (2001) 195121.
[20] J.W. Clark, in: D. Wilkinson (Ed.), Progress in Particle and Nuclear Physics, vol. 2, Pergamon Press, Oxford, 1979, p. 89ff.
[21] G. Ripka, Phys. Rep. 56 (1979) 1.
[22] J.G. Zabolitzky, Phys. Rev. A 16 (1977) 1258.
[23] M. Gaudin, J. Gillespie, G. Ripka, Nucl. Phys. A 176 (1971) 237.
[24] E. Krotscheck, Nucl. Phys. A 293 (1977) 293.
[25] R. Lustig, Mol. Phys. 55 (1985) 305.
[26] R. Zucker, in: M. Abramowitz, I.A. Stegun (Eds.), Handbook of Mathematical Functions, U.S. Government Printing Office, Washington, 1972 (equation 4.4.33).
[27] Q.N. Usmani, B. Friedman, V.R. Pandharipande, Phys. Rev. B 25 (1982) 4502.
[28] R.A. Smith, A. Kallio, M. Puoskari, P. Toropainen, Nucl. Phys. A 328 (1979) 186.
[29] V.R. Pandharipande, H.A. Bethe, Phys. Rev. C 7 (1973) 1312.
[30] H.W. Jackson, E. Feenberg, Ann. Phys. 15 (1961) 266.
[31] S. Chakravarty, C.-W. Woo, Phys. Rev. B 13 (1976) 4815.
[32] F.W.J. Olver, in: Handbook of Mathematical Functions, op. cit. (section 9.9).
[33] W.H. Press, S.A. Teukolsky, W.T. Vetterling, B.P. Flannery, Numerical Recipes in FORTRAN, second ed., Cambridge University Press, Cambridge, 1992 (section 4.3).
[34] J.W. Clark, P. Westhaus, Phys. Rev. 141 (1966) 833;
Phys. Rev. 149 (1966) 990.
[35] See, for example, T.H. Hill, Statistical Mechanics, Dover, New York, 1956.